European Polymer Journal 195 (2023) 112203

Contents lists available at ScienceDirect

European Polymer Journal

journal homepage: www.elsevier.com/locate/europolj

Thiol-ene photopolymerization meets azide-alkyne click reactions: P/N/Si-containing, dual curable eugenol-based hybrid coatings

Ozge Ozukanar [a], Emrah Çakmakçi [b,*], Ozgun Daglar [a], Hakan Durmaz [a], Volkan Kumbaraci [a,*]

[a] Department of Chemistry, Istanbul Technical University, 34469 Istanbul, Turkey
[b] Department of Chemistry, Marmara University, 34722 Istanbul, Turkey

ARTICLE INFO

Keywords:
Green chemistry
Thiol-ene photopolymerization
Eugenol
Azide-alkyne click
Dual-curing

ABSTRACT

The use of bio-based building blocks for the synthesis of polymers is increasing day by day. Among the bio-based building blocks, eugenol is a highly promising monomer for the preparation of thermoset materials. In this study, we combined thiol-ene photopolymerization (TEP) and thermal azide-alkyne cycloaddition click reactions to prepare eugenol-based thermally stable, P-, N-, and Si-containing networks. To this end, we synthesized a P-containing, eugenol-based monomer bearing azide group and a siloxane compound containing an alkyne group. By mixing these monomers with multifunctional thiols and by utilizing a dual-curing strategy, we managed to obtain optically transparent and thermally stable coatings with excellent adhesion to glass substrates. Thermal stability, optical transmittance, pendulum hardness, solvent resistance, and the adhesion performance of the coatings were evaluated. The gel contents of the thermoset materials were found to be over 95%. At 600 °C, the char yields of the dual-cured coatings were found to be over 30%. Coatings were also found to be resistant to acidic and basic conditions as well as solvents.

1. Introduction

Photopolymerization, which has numerous applications ranging from 3D printers to coatings, is a radical-induced process and can be simply described as the transfer of suitable monomers/oligomers (acrylate, methacrylate, vinyl compounds, etc.) into polymers within seconds with the aid of light and in the presence of compounds known as photoinitiators (PI) [1–8]. Upon light illumination that matches the absorption wavelength range of the PI dissolved within the monomers, the PI absorbs photons and decomposes to give radical species that initiate the free-radical polymerization. Some PIs also generate H^+ cations, which effectively polymerize vinyl, epoxy, or oxetane compounds. Photopolymerization is often regarded as an environmentally friendly method for its low energy consumption, high curing speed, solvent-free nature, and low to zero VOC (volatile organic compound) emissions [8,9].

However, photopolymerization suffers from a few drawbacks. Among them, the oxygen inhibition effect is the most important one; it causes tacky surfaces and leads to low monomer conversion values. Many techniques such as curing under nitrogen atmosphere, using high photoinitiator loadings, wax addition, increasing light intensity, etc., have been suggested to overcome the oxygen inhibition effect in photopolymerization [10,11]. Nonetheless, an alternative, superior photopolymerization method, namely thiol-ene photopolymerization (TEP) has hit the scene in the last decade. TEP not only overcomes the oxygen inhibition effect but also brings unique features such as photoinitiatorless-curing, higher percentages of monomer conversion, low shrinkage, homogeneous network formation, etc. [12–14]. Besides, TEP enables the polymerization of allylic monomers which tend to form dimers or oligomers and do not undergo homopolymerization via free radicals [15]. In the TEP method, multifunctional thiols and allylic compounds (acrylates, methacrylates, maleimides, etc., can also be used) are used, thiyl radicals are generated upon irradiation and are added to the allyl double bonds in an anti-Markovnikov fashion and the polymer chains form by stepwise addition reactions, leading to thioether bonds. Therefore, TEP is known to proceed via a radical-induced step-growth mechanism [16–18].

TEP offers an excellent solution to prepare tack-free coatings. The versatility of the commercially available thiols and double bond-containing monomers used in TEP allows the design of coatings and polymers with tunable thermal, optical, and mechanical properties. Nevertheless, most of the suitable double bond-containing monomers

* Corresponding authors.
E-mail addresses: emrah.cakmakci@marmara.edu.tr (E. Çakmakçi), kumbaracii@itu.edu.tr (V. Kumbaraci).

https://doi.org/10.1016/j.eurpolymj.2023.112203
Received 4 April 2023; Received in revised form 25 May 2023; Accepted 31 May 2023
Available online 5 June 2023
0014-3057/© 2023 Elsevier Ltd. All rights reserved.

are toxic and depend on petroleum sources. Moreover, even though the thermal and mechanical properties can be tailored, often TEP leads to relatively low mechanical properties and low glass transition temperatures (T_g) due to the presence of flexible thioether bonds [19]. TEP-based networks are also flammable due to the nature of the common monomers used in TEP, which are composed of C, H, O, and S elements.

To overcome the above-mentioned problems of TEP-based thermoset coatings, various approaches have been suggested in the literature. For instance; in line with the goals of the "Green Chemistry" concept, the use of bio-based building blocks instead of fossil-based monomers has become an intriguing area of research [20,21]. Methods such as the preparation of nanocomposite or hybrid materials and the use of rigid monomers are frequently applied to improve the mechanical properties of TEP-based networks [22]. In addition, flame retardant reactive monomers containing B/P/N/Si are often used to impart flammability resistance. [15,19,22–25]. However, it is challenging to combine two or more of these elements in a single molecule containing reactive functional groups, yet it is an effective approach to achieve flame retardant monomers with good flame resistance, combining and revealing the synergistic effect of these elements.

Eugenol, which is usually obtained from clove, cinnamon, and basil, is a unique bio-based compound among many other bio-based building blocks, comprising allyl and phenol functional groups [26–28]. The inherent presence of an allyl group in eugenol eliminates the need for derivatization with toxic allylating agents such as allyl bromide which is generally utilized for the introduction of allyl groups to other bio-based building blocks such as pyrogallol, isosorbide, etc. [29,30].

Here, we prepared a P-containing, eugenol-based monomer having azide groups (PEECH-N_3) and an alkyne-functional siloxane compound (PAS) and reacted these two compounds via copper-catalyzed azide-alkyne cycloaddition (CuAAC) click reactions to prepare a novel reactive, flame-retardant monomer comprising P, N, and Si elements. Nevertheless, the yield of this newly prepared monomer was found to be low. Therefore, we utilized a dual-curing strategy to prepare eugenol-based coatings. We first conducted the thiol-ene photopolymerization and reacted PEECH-N_3 and PAS with multifunctional thiols, and then heated the coatings to thermally activate the click reactions between the propargyl and azide-functional groups. Previously, thiol-ene/yne photochemical functionalization/ photopolymerization and azide-alkyne click reactions were used together to prepare linear polymers [31–33], hyperbranched polymers [34], dendrimers [35], gels [36] and functional micro/nanoparticles [37,38], etc. There are examples in the literature where coatings were prepared via TEP by using a monomer which was synthesized by using an azide-alkyne click reaction [19,23]. Previously, the thiol-Michael addition reaction was combined with photo-induced CuAAC to prepare thermoset materials with wrinkled surfaces [39]. However, to our best knowledge, TEP and azide-alkyne click polymerization techniques were not previously combined in a dual-curing fashion to prepare coatings. The originality of this work not only stems from the newly synthesized monomers but also from this dual-curing strategy.

2. Experimental

2.1. Materials

Ethanol (EtOH), sodium azide (NaN_3), dichloromethane (CH_2Cl_2), anhydrous sodium sulfate (Na_2SO_4), phenylphosphonic dichloride, chloroform ($CHCl_3$), triethyl amine (Et_3N), hexane, propargyl alcohol, 3-isocyanatopropyltriethoxy silane (ICTES), *N*,*N*-dimethylformamide (DMF), *N*,*N*,*N*′,*N*′′,*N*′′-pentamethyldiethylenetriamine (PMDETA), copper(I) bromide (CuBr), neutral alumina, trimethylolpropane tris(3-mercaptopropionate) (3SH), pentaerythritol tetrakis(3-mercaptopropionate) (4SH), phenylbis(2,4,6-trimethylbenzoyl) phosphine oxide (BAPO), hydroxy-2-methylpropiophenone (Darocur 1173), dibutyltin dilaurate (DBTDL) methyl ethyl ketone (MEK), and acetone were purchased from Sigma Aldrich. All solvents were of HPLC or ACS grade. Magnesium sulfate anhydrous and 4 Å molecular sieves were used as drying agents. Purifications via column chromatography were performed with silica gel 60 (Merck, 0.040–0.063 mm) which has 230–400 mesh ASTM and Celite®. Analytical thin layer chromatography (TLC) was performed on Merck labeled silica gel (60 HF254, 90%<55 μm) plates (0.25 mm) precoated with a fluorescent indicator. Visualization was affected with 254 nm ultraviolet light and iodine on silica.

2.2. Characterization methods

Proton nuclear magnetic resonance (^{1}H NMR) measurements were recorded in $CDCl_3$ using an Agilent VNMRS (500 MHz) instrument. Chemical data for protons are reported in parts per million (ppm, scale) downfield from tetramethylsilane and are referenced to the residual proton in the NMR solvent ($CDCl_3$: δ 7.26). The chemical shifts δ are reported in parts per million (ppm) as follows: chemical shift, multiplicity (s = singlet, d = doublet, t = triplet, q = quartet, m = multiplet, br = broad), coupling constant J (expressed in Hertz). The carbon nuclear magnetic resonance (^{13}C NMR) spectra were recorded at Agilent VNMRS (125 MHz). FT-IR spectra were recorded on an Agilent Technologies Cary 630 FT-IR instrument over the range of 4000–500 cm^{-1}. Ultra Performance Liquid Chromatography measurements (UPLC-QTof) were performed by using Waters (Acquity H Class Plus) UPLC instrument equipped with Vion IMS QTof. Thermogravimetric analyses (TGA) of the photocured films were performed by using a PerkinElmer thermogravimetric analyzer (Pyris 1 TGA model). Samples were run from 30 to 600 °C with a heating rate of 10 °C/min under a nitrogen atmosphere. Differential scanning calorimetry (DSC) was performed on PerkinElmer Diamond DSC from 30 to 180 °C with a heating rate of 10 °C min^{-1}. Gel contents were determined by immersing the pre-weighted samples in acetone for 24 h. The insoluble gel fraction was dried in a vacuum oven at 40 °C to constant weight and the gel percentage was calculated. The wettability characteristics of the coatings were performed on a Kruss (Easy Drop DSA-2) tensiometer. The contact angles (h) were measured using the sessile drop test method in which drops were created using a syringe. Measurements were made using 3–5 μl of distilled water. For each sample, at least five measurements were made, and the average value is reported. The gloss (ASTM D-523–80), pencil hardness (ASTM D-3363), cross-cut (DIN 53151), and MEK rub tests (ASTM D-5402) were conducted according to the indicated standard test methods. Water absorption percentages of the coatings were calculated by measuring the weight gain of the test specimens after being immersed in water for 24 h. Theoretical limiting oxygen index (LOI) calculations were conducted by using the char residue percentages obtained at 600 °C and according to the following equation [40]:

$$LOI = 17.5 + 0.4x\%residueat600^{\circ}C \quad (1)$$

2.3. Synthesis of EECH-N_3

The synthesis of EECH-N_3 was carried out according to the literature [41]. First, Eugenol glycidylether (EECH, Scheme 1a) was prepared according to the literature [42,43]. EECH (1 eq., 4 g, 18.16 mmol) was dissolved in EtOH (80 mL) in a 250 mL round-bottom flask. Then, NaN_3 (3 eq., 3.54 g, 54.48 mmol) was dissolved in 90 mL water and added to the EECH solution via a dropping funnel, and the reaction mixture was stirred overnight at room temperature. The mixture was taken to a separatory funnel and extracted three times with CH_2Cl_2. All organic phases were collected, dried with Na_2SO_4, and the solvent was evaporated under reduced pressure to give the product as a viscous yellow liquid (yield: 4.06 g, 96%). The synthesis of EECH-N_3 is shown in Scheme 1b.

^{1}H NMR (500 MHz, $CDCl_3$, δ): 6.87 (d, 1H, Ar), 6.73 (d, J = 7.6 Hz, 2H, Ar), 5.95 (m, 1H, C = CH), 5.07 (m, 2H, C = CH_2), 4.15 (m, 1H, OCH_2), 4.07 (m, 1H. OCH_2), 4.01 (m, 1H, CHO), 3.85 (s, 3H, OCH_3),

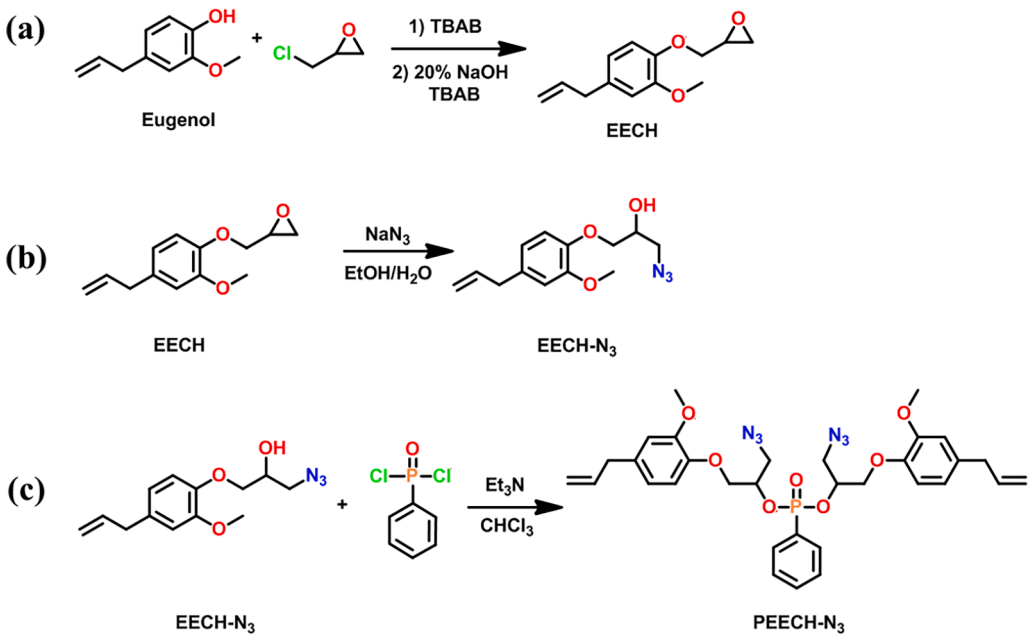

Scheme 1. The synthetic route to EECH (a), EECH-N_3 (b), and PEECH-N_3 (c).

3.48 (m, 2H, CH_2N_3), 3.33 (d, J = 6.7 Hz, 3H, $ArCH_2$ and OH).

^{13}C NMR (125 MHz, $CDCl_3$, δ): 149.76, 146.16, 137.44, 134.54, 120.84, 115.84, 115.63, 112.48, 76.88, 71.98, 69.30, 55.83, 53.89, 53.19, 39. 84.

FT-IR (cm^{-1}): 3446, 3075, 2931, 2097, 1638,1589,1507,1459, 1418, 1258, 1226, 1138, 1028.

2.4. Synthesis of PEECH-N_3

Into a 50 mL of two-necked round-bottom flask, phenylphosphonic dichloride (1 eq., 0.34 g, 1.73 mmol) was dissolved in 20 mL of $CHCl_3$ and the solution was cooled to 0 °C using an ice bath. Then, the mixture of EECH-N_3 (2.2 eq., 1.00 g, 3.80 mmol) and Et_3N (2.5 eq., 0.6 mL, 4.32 mmol) in 5 mL of $CHCl_3$ was added to the solution dropwise under nitrogen. After the addition was completed, the mixture was allowed to stir at 0 °C for 30 min and overnight at room temperature. The solution was washed with water, dried with Na_2SO_4, and the solvent was evaporated under reduced pressure. Finally, the crude product was dissolved in a little amount of $CHCl_3$ and precipitated into hexane to give the product as a yellow viscous liquid (yield = 0.71 g, 63.4%). The synthesis of PEECH-N_3 is shown in Scheme 1c.

^{1}H NMR (500 MHz, $CDCl_3$, δ): 7.79 (m, 2H, Ar), 7.43 (m, 3H, Ar), 6.80 (d, J = 8.1 Hz, 2H, Ar), 6.69 (m, 4H, Ar), 5.91 (m, 2H, C = CH), 5.03 (m, 4H, C = CH_2), 4.13 (m, 3H, OCH_2), 3.98 (dd, J = 5.5, 1.4 Hz, 3H, OCH_2 and OCH), 3.79 (s, 6H, OCH_3), 3.45 (dd, J = 14.4, 5.3 Hz, 4H, CH_2N_3), 3.30 (d, J = 6.7 Hz, 4H, $ArCH_2$).

^{13}C NMR (125 MHz, $CDCl_3$, δ): 149.63, 146.26, 137.49, 134.11, 132.51, 131.76, 128.46, 128.00, 120.74, 115.75, 115.09, 112.45, 77.29, 71.47, 69.15, 55.78, 53.39, 39.81.

FT-IR (cm^{-1}): 3362, 3058, 2935, 2495, 2096, 1638, 1589, 1507, 1440, 1418, 1395, 1259, 1228, 1131, 1030, 941, 915.

ESI-MS, m/z $C_{32}H_{37}N_6O_7P$ calculated: 648.25; Found: 649.25426 $[M + H]^+$.

2.5. Synthesis of propargyl alkyl silane (PAS)

The synthesis was performed according to the literature [44]. Into a 50 mL of two-necked round bottom flask, propargyl alcohol (1.2 eq., 1.26 mL, 21.83 mmol) and Et_3N (1 eq., 2.56 mL, 18.19 mmol) were dissolved in 10 mL of $CHCl_3$, and the mixture was cooled to 0 °C in an ice bath. The solution of ICTES (1 eq., 4.55 mL, 18.19 mmol) in 5 mL of $CHCl_3$ was added to this mixture dropwise under nitrogen. After the addition was completed, the mixture was allowed to stir at 0 °C for 30 min and overnight at room temperature. The solution was washed with water, dried with Na_2SO_4, and the solvent was evaporated under reduced pressure. The product was obtained as an orange oil (yield = 4.52 g, 81.9 %). The structure of PAS can be seen in Scheme 2.

^{1}H NMR (500 MHz, $CDCl_3$, δ): 5.22 (bs, 1H, NH), 4.60 (d, J = 2.5 Hz, 2H, OCH_2), 3.75 (q, J = 7.0 Hz, 6H, $SiOCH_2$), 3.13 (m, 2H, CH_2N), 2.43 (t, J = 2.5 Hz, 1H, C≡CH), 1.57 (m, 2H), 1.17 (t, J = 7.0 Hz, 9H, CH_3), 0.57 (m, 2H, $SiCH_2$).

^{13}C NMR (125 MHz, $CDCl_3$, δ): 155.45, 78.39, 74.38, 58.36, 52.15, 43.44, 23.10, 18.18, 7.52.

FT-IR (cm^{-1}): 3308, 2972, 2910, 2885, 2126, 1707, 1526, 1442, 1390, 1250, 1099, 1071, 952.

2.6. Synthesis of STBEPP via azide-alkyne click reaction

Into a 250 mL round-bottom flask, PEECH-N_3 (1 eq., 1.80 g, 2.77 mmol) dissolved in dry DMF (10 mL). Next, PAS (2.10 eq., 1.77 g, 5.83 mmol), PMDETA (0.40 eq., 192.37 mg, 1.11 mmol), and CuBr (0.40 eq., 159.23 mg, 1.11 mmol) were added to this solution, respectively. After 3 freeze–pumpthaw cycles, the mixture was left to stir at room temperature for 24 h. The reaction mixture was filtered through a neutral alumina column using CH_2Cl_2 as an eluent. Then, all collected organic phases were extracted three times with water, dried with Na_2SO_4, filtered, and evaporated to dryness. The pure product was obtained by precipitating the crude product into hexane (yield: 0.7 g, 20 %). The synthesis of STBEPP is depicted in Scheme 2.

^{1}H NMR (500 MHz, $CDCl_3$, δ): 7.81–7.30 (m, 5H, Ar), 7.20–6.71 (m, 8H, Ar), 5.92 (m, 2H, C = CH), 5.18 – 4.37 (m, 18H), 3.97 (m, 19H, OCH_3 and $SiOCH_2$), 3.35 (d, J = 6.7 Hz, 4H, $ArCH_2$), 3.18 (q, J = 6.7 Hz, 4H, CH_2N), 1.60 (p, J = 7.2 Hz, 4H,), 1.20 (t, J = 7 Hz, 18H, CH_3), 0.61 (t, J = 8.3 Hz, 4H, $SiCH_2$).

^{13}C NMR (125 MHz, $CDCl_3$, δ): 162.54, 156.20, 155.47, 149.77, 146.51, 145.96, 143.40, 137.51, 137.35, 134.72, 133.98, 132.38, 131.77, 131.69, 129.06, 128.51, 128.40, 128.39, 125.23, 120.79, 115.88, 115.26, 112.45, 77.33, 74.38, 71.73, 71.29, 69.01, 68.78, 66.87, 62.12, 58.43, 55.78, 53.78, 52.74, 52.22, 43.43, 39.80, 36.45, 31.40, 23.21, 18.24, 16.31, 15.08, 14.63, 7.57.

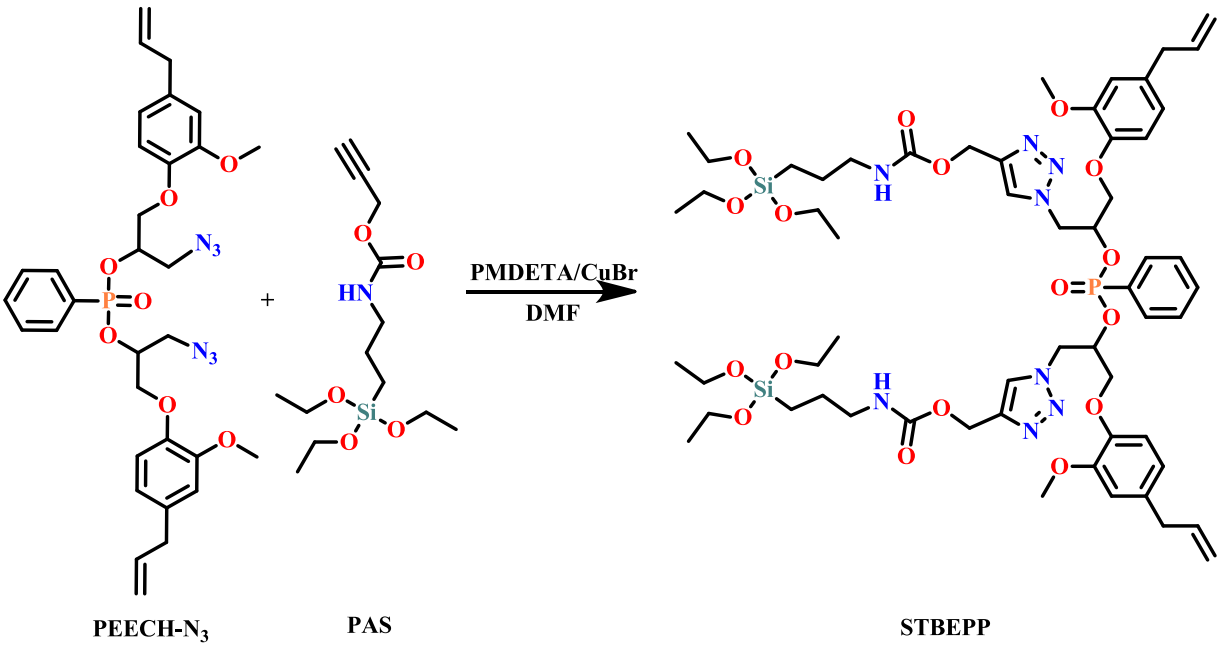

Scheme 2. The synthetic route to STBEPP.

FT-IR (cm^{-1}): 3317, 2972, 2924, 1716, 1668, 1511, 1440, 1388, 1231, 1073, 1019, 920.

ESI-MS, *m/z* $C_{58}H_{87}N_8O_{17}PSi_2$ calculated: 1254.5465; Found: 1255.5543 $[M + H]^+$.

2.7. Preparation of thermoset coatings via dual-curing

Here, STBEPP was not utilized for the preparation of the coatings due to its low yield (see discussion). Instead, we prepared two different coating formulations (Table 1) and applied a dual-curing system. We first mixed PEECH-N_3 and PAS with the multifunctional thiol (either 3SH or 4SH). Then, 1 wt% BAPO and 3 wt% Darocur 1173 were added. The mixture was stirred at 60 °C for about 15 min until solid BAPO was completely dissolved and a homogeneous mixture was obtained. During this procedure, the solution was kept away from being exposed to light to prevent polymerization. Next, 2 wt% DBTDL and a drop of water were added to this mixture and the solution was placed into a vacuum oven to remove dissolved oxygen within the mixture (degassing). Finally, the solutions were coated on glass substrates. The coatings were cured under UV light for about 5 min. Then, the coated glass substrates were transferred to an oven and heated from room temperature to 120 °C with a heating rate of 10 °C/min. This post-thermal curing step was continued for 2 h. Similarly, we prepared free films by pouring the liquid mixtures into Teflon molds (50x10x1 mm) and cured them as described above. The dual-curing approach is depicted in Scheme 3.

Table 1
Composition of the coatings.[a]

	PEECH-N_3	PAS	3SH[b]	4SH[b]	Gel content (%)[c]
TD3SH	4 mmol	8 mmol	3.2 mmol	–	96 (58)
TD4SH	4 mmol	8 mmol	–	2.4 mmol	95 (56)

[a] 1 wt% BAPO, 3 wt% Darocur 1173, 2 wt% DBTDL, and a drop of water were added to each formulation.

[b] Thiols were taken 1.2 M excess of the molar amount of the allyl functionality.

[c] The numbers in parenthesis display the gel content values before thermal treatment.

3. Results and discussion

3.1. Characterization of the monomers

Here, we aimed to prepare a P-, N-, and Si-containing novel difunctional monomer (STBEPP) to be used for thiol-ene photopolymerization applications. First, azide and hydroxyl functional EECH-N_3 was prepared through the ring-opening reaction of EECH. EECH-N_3 was synthesized in excellent yield (96%) and characterized by FTIR and NMR techniques. The ^{1}H NMR of EECH-N_3 is presented in Fig. 1. The allylic protons of the eugenol moiety resonated between 6.0 and 5.0 ppm while the aromatic protons were observed between 7.0 and 6.0 ppm. The hydrogens of the methoxy group were detected as a singlet at 3.85 ppm. The –OH proton signal (h) and the signals of the protons of the methylene unit (c) between the aromatic ring and the double bond overlapped at 3.33 ppm. The NMR signals belonging to the epoxide group of EECH were transformed after the ring-opening reaction, the formerly present NMR signals at 2.86 and 2.71 ppm disappeared after the reaction. The other protons were also found to be in good accordance with the structure of the target compound as marked in Fig. 1. Moreover, the structure of EECH-N_3 was confirmed via ^{13}C NMR (Figure S1).

The FTIR spectrum of EECH-N_3 is given in Figure S2. The broad band at around 3446 cm^{-1} in the FTIR spectrum of EECH-N_3 was attributed to the –OH stretching vibrations and the band at 3075 cm^{-1} was due to the aromatic -C–H vibrations. Also, the allylic double bond vibration band was detected at 1638 cm^{-1} and the characteristic azide (-N = N = N-) stretching band was also observed at around 2100 cm^{-1}. Besides, it is seen from this spectrum that the bands related to the oxirane ring of EECH at 840 and 760 cm^{-1} were absent, indicating that the epoxide rings were reacted [42].

Next, we reacted EECH-N_3 with phenylphosphonic dichloride in $CHCl_3$ to obtain PEECH-N_3. Previously, eugenol was directly reacted with phosphorus oxychloride to give a similar phosphorous compound; trieugenylphosphate [45]. The ^{1}H NMR and ^{13}C NMR spectra of PEECH-N_3 are given in Fig. 2 and Figure S3, respectively. The ^{1}H NMR spectrum of PEECH-N_3 displays that all the peaks associated with the structure of EECH-N_3 were preserved except for the –OH proton (h) signal at around 3.33 ppm. Before the reaction, the integral ratio of the double bond to the signal at 3.33 ppm (c + h protons) was (3.01/2.94) ~ 1. In the ^{1}H NMR spectrum of PEECH-N_3, this ratio was found as (6.06/4.15) ~ 1.5,

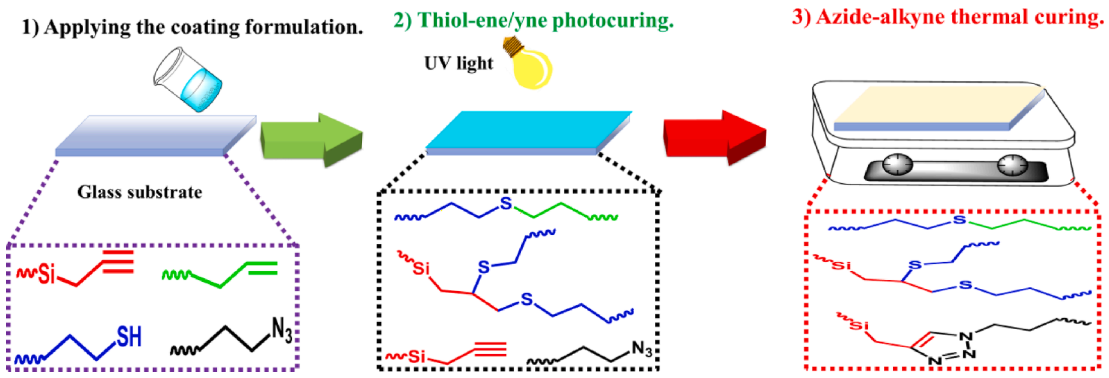

Scheme 3. The illustration of the dual-curing approach. For clarity, only the functional groups are depicted. In the first stage, thiol groups react with the allyl and alkyne functionalities. The remaining alkyne units then react with the azide groups upon thermal treatment. Finally, crosslinked hybrid coatings are obtained.

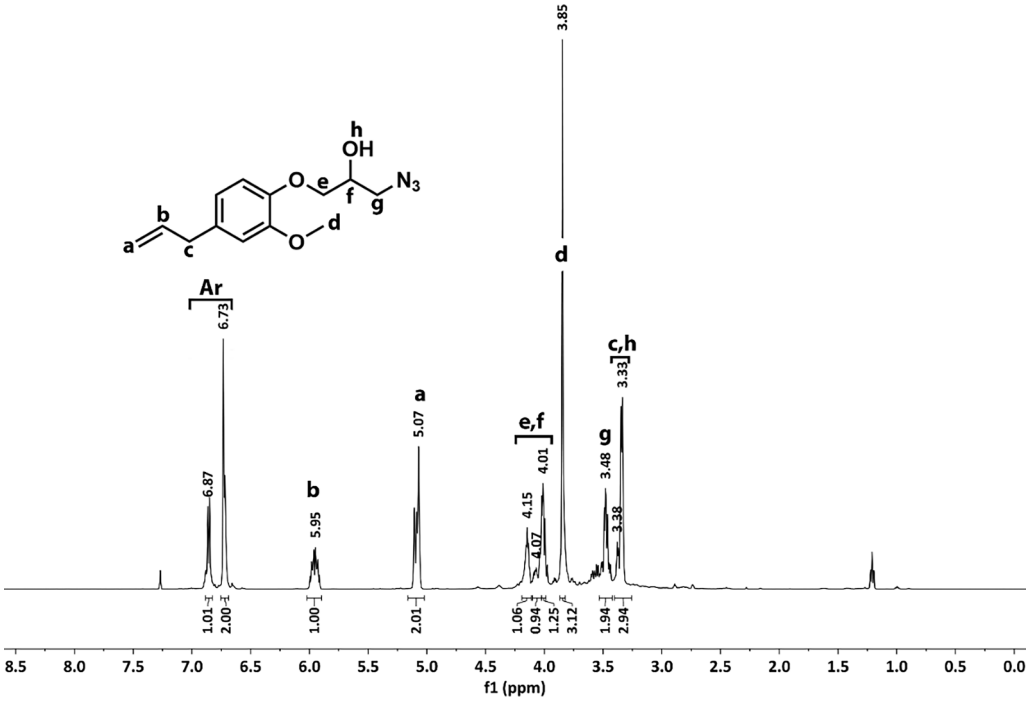

Fig. 1. The ^{1}H NMR of EECH-N_3 in $CDCl_3$ (500 MHz).

as expected. Additionally, new signals at around 8.0–7.0 ppm were observed in the ^{1}H NMR spectrum of PEECH-N_3 belonging to the aromatic protons arising from the phenylphosphonic group. The ^{13}C NMR spectrum of PEECH-N_3 (Figure S3) was also recorded and found to further confirm its structure.

The FTIR spectrum of PEECH-N_3 was presented in Figure S4 and found to be different than the FTIR spectrum of EECH-N_3. The broad band associated with the –OH bond vibration was disappeared in the FTIR spectrum of PEECH-N_3. Besides new bands appeared at 1131 cm^{-1} and 1030 cm^{-1} which were attributed to the –P = O and –P-O-C stretching vibrations, respectively.

The propargyl alkyl silane (PAS) was synthesized by using slightly excess propargyl alcohol and ICTES and characterized by ^{1}H NMR, ^{13}C NMR, and FTIR techniques. In the H NMR of PAS (Fig. 3), the CH_3– protons were detected as a triplet at 1.17 ppm while the -CH_2OSi- protons were found to resonate at 3.75 ppm. The methylene protons attached directly to the Si atom (-CH_2Si) were observed at 0.57 ppm. The ^{1}H NMR signal for the proton of the alkyne unit (≡CH) was detected as a singlet peak at 2.43 ppm. Other protons were observed between 5.0 and 2.0 ppm, accordingly. Finally, the –NH proton in the urethane linkage was found to resonate at 5.22 ppm. The structure of PAS was further confirmed via ^{13}C NMR (Figure S5). Additionally, the FTIR spectrum of PAS was recorded and presented in Figure S6. The band at 3308 cm^{-1} in the FTIR spectrum of PAS was attributed to the –NH stretchings and the alkyne ≡C-H vibrations while the band at 1707 cm^{-1} was due to characteristic urethane carbonyl vibrations. Finally, the absence of the –NCO stretching vibration band at around 2270 cm^{-1} in the FTIR spectrum of PAS further confirmed and proved that the reaction was carried out successfully.

Subsequently, we tried to synthesize a P-, N-, and Si-containing eugenol-based reactive monomer (STBEPP) by reacting PEECH-N_3 and PAS using the well-known CuAAC click reaction. Regardless of our several trials optimizing the reaction conditions for the maximum yield, the yield of STBEPP was found to be as low as 20%. We attributed this situation to the hydrolysis of the PAS during the click reaction leading to several side products and decreasing the yield of the target compound. We must also note that PAS alone is not very stable and should be stored under nitrogen gas (or under vacuum) in a refrigerator. Nevertheless, we characterized STBEPP via NMR, FTIR, and mass spectroscopy techniques. The ^{1}H NMR of STBEEP is given in Fig. 4. The signals between

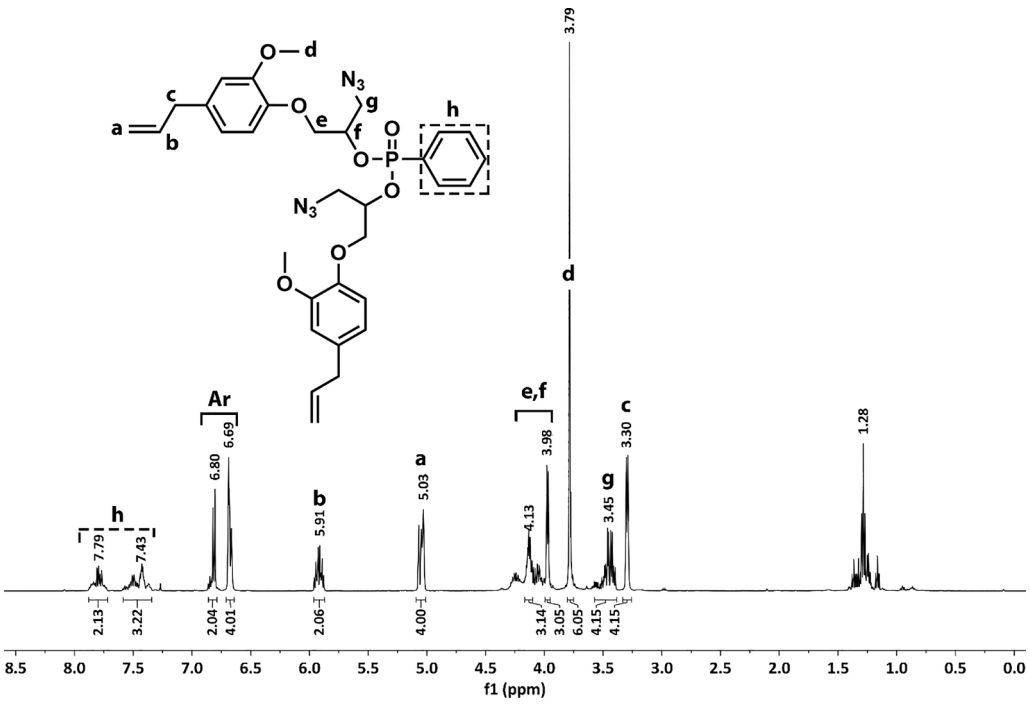

Fig. 2. The ^{1}H NMR of PEECH-N_3 in $CDCl_3$ (500 MHz).

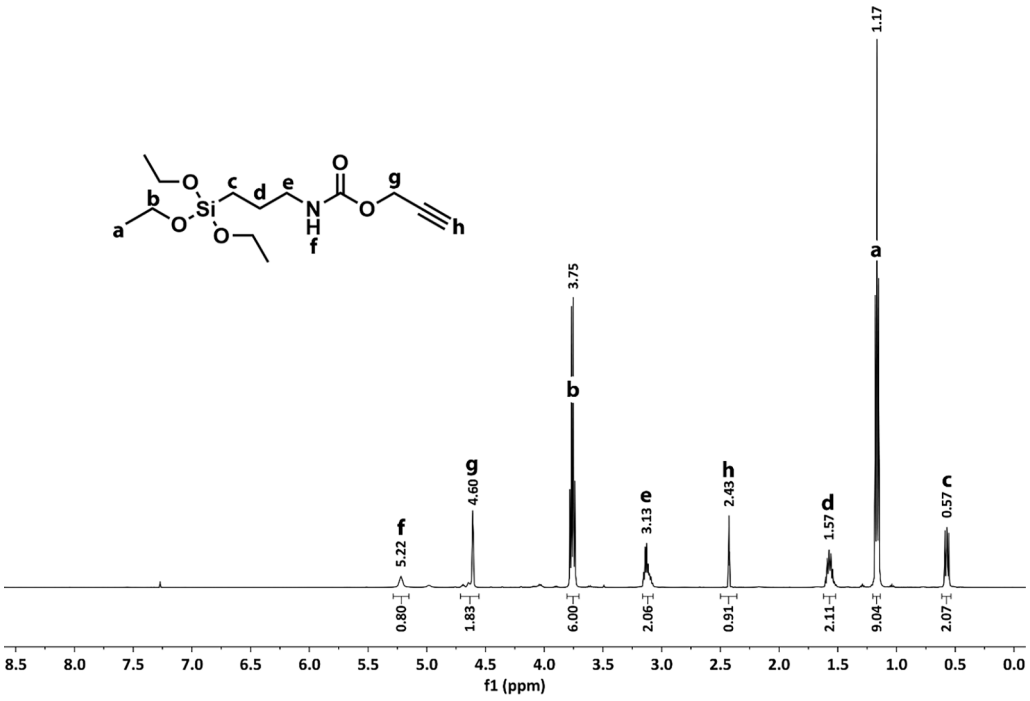

Fig. 3. The ^{1}H NMR of PAS in $CDCl_3$ (500 MHz).

8.0 and 6.5 ppm were attributed to the aromatic protons as well as to the protons of the newly formed triazole rings. The absence of the NMR signal belonging to the alkyne (≡CH) groups at 2.43 ppm is a direct evidence showing that the click reaction was successful. The ^{13}C NMR of STBEPP is given in Figure S7. The ^{13}C NMR of STBEPP confirms its structure. The FTIR spectrum of STBEPP (Figure S8) does not display alkyne or azide bands at around 2100–2300 cm^{-1} which proves that the click reaction was successful. The mass of STBEPP was also verified by mass spectrometry which showed that the *m/z* ratio of STBEPP is 1255.5543 $[M + H]^{+}$ (theoretical mass 1254.5465) indicating high purity. The mass spectra of PEECH-N_3 and STBEPP are given in Figures S9 and S10.

3.2. Physical appearance of the coatings

Due to the low yield of STBEPP, we preferred not to use it in our coating formulations but we found an elegant way to in-situ synthesize STBEPP by combining TEP and thermal azide-alkyne click reaction. For this purpose, first, we mixed PEECH-N_3, PAS, a multifunctional thiol compound (3SH or 4SH), and photoinitiators and cured this mixture

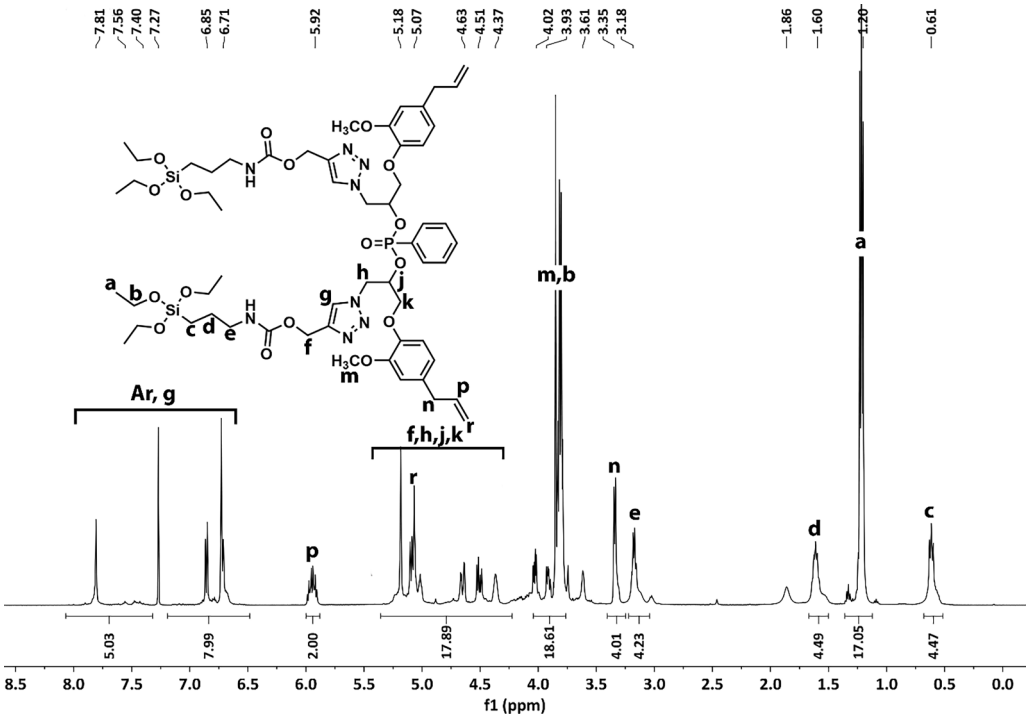

Fig. 4. The ^{1}H NMR of STBEPP in $CDCl_3$ (500 MHz).

under UV light, and then in the next stage, the azide-alkyne click reaction was triggered via heating. Generally, a 1:1 ratio of ene/yne to thiol ratio is preferred in thiol-ene/yne photopolymerization systems. For instance, in our case, the total amount of the required thiol functional groups is 24 mmol (8 mmol of 3SH) for 8 mmol of allyl groups coming from 4 mmol of PEECH-N_3 plus 16 mmol of reactive groups coming from 8 mmol of PAS. We hypothesized that the reactivity of alkenes would be higher in TEP with respect to the alkyne groups. Thus, here, we used less amount of the thiol component that is needed to react with the double and triple bonds in order to have unreacted triple bonds after the first stage of curing. Thereby, we presumed that unreacted alkyne groups would be present within the partially polymerized mixture after the first curing step and these unreacted triple bonds would react with the azide groups in the second stage. Nevertheless, we took a slightly excess amount of the thiol compound that is required to convert all the allylic double bonds of PEECH-N_3 to make sure a relatively crosslinked polymer matrix is achieved after the first stage.

During the first stage, both alkene and alkyne groups react photochemically with the thiol compound under UV light. However, as noted above we anticipated that the double bonds would react faster than the triple bonds, (leading unreacted PAS). Theoretical calculations of the reactivity of alkenes and alkynes in thiol-x photochemical reactions (x stands for -ene or -yne) were previously determined [46,47]. Depending on the type of the ene/yne, both species react with thiyl radicals. One interesting feature of alkynes is that they react in two steps; where the second step is three times faster than the first step [48]. In the first step, vinyl sulfide monomer forms which then rapidly reacts with another thiyl radical. To our best knowledge, the reactivity of these two species in a mixture or in a single molecule such as 1-pentene-4-yne was not evaluated. On the other hand, it was reported that alkynes are less reactive in radical reactions [49,50]. Compared to alkynes, the addition of a methyl radical to an alkene was found to be faster despite the greater exothermicity of the alkynes. The reason for this peculiar behavior of alkynes was attributed to their larger singlet–triplet band gap, leading to a high reaction energy barrier. Additionally, it was previously shown that most of the acetylene groups remain unreacted when propargyl acrylate which bears both alkyne and acrylic double bond, is subjected to free radical polymerization [51,52]. Although all these previous studies support our view that alkenes and alkynes used in TEP are selective and most of the propargyl groups remained unreacted in the first step of our curing schedule, the reactivity of alkene and alkynes towards thiyl radicals needs to be further explored. Nevertheless, even if all the triple bonds were reacted in the first stage, alkene double bonds are also known to react with the azide groups via heating [53–55]. Thus, via either two routes (azide–alkyne or azide-alkene) fully crosslinked systems could be prepared with the applied dual-curing method.

After UV curing, both the free films and the coatings had mushy appearances with soft, tacky surfaces that could be attributed to the low degree of conversion and unreacted alkyne, allyl, and azide units. The tackiness of the coatings can also be attributed to the low reactivity of the allyl group in eugenol, which leads to incomplete thiol-ene reactions due to the stabilization of radicals via resonance [56–57]. After storing the free films at room temperature for about two weeks, the films became tack-free and relatively tough (Fig. 5a, i). These free films were yellow in color and many pores formed during storage. The porosity formation and the hardening were attributed to the formation of siloxane-based crosslinked structures via the hydrolysis and condensation reactions of the PAS within the polymer network.

On the other hand, thermally treated free films were brown in color which was ascribed to the formation of triazole rings (Fig. 5a, ii). Again, porous, foam-like free films were obtained, yet the thermally cured-free films were highly rigid and brittle when tried to be bent as opposed to the room-temperature stored-free films which could be bent without breaking (Fig. 5b). This finding shows that the thermal curing catalyzed both the azide-alkyne click reactions and the siloxane network formation. Notably, 3–4% weight loss occurred after the thermal curing procedure which might be attributed to the loss of ethanol as a result of the hydrolysis and condensation reactions between the alkoxysilane groups.

The coatings applied on glass surfaces were colorless or yellow depending on the thickness of the coatings (Fig. 5c-g). Due to the large surface area and the relatively lower thickness of the coatings (<100 μm), the porous structures were not formed. Colorless to yellow-colored film formation can be seen in the examples given in the literature where eugenol-based thiol-ene photocured coatings were prepared [56,58].

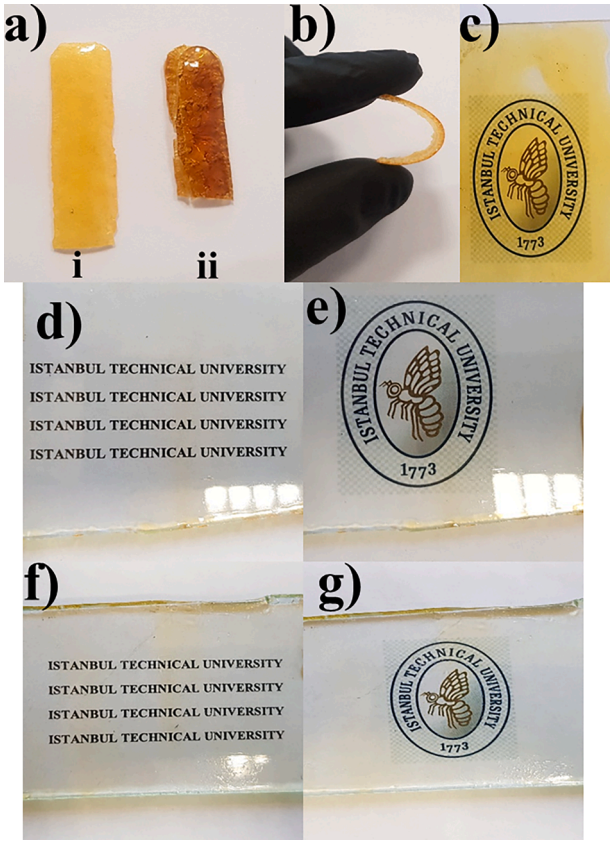

Fig. 5. The digital images of the free films of TD3SH (a and b), the glass substrates coated with TD3SH formulation (d and e), and the glass substrates coated with TD4SH formulation (f and g). The image on (c) displays a thick coating of TD3SH formulation. The photocured and room temperature aged sample (i) can be bent (b) while dual-cured films were highly rigid and cannot be bent without breaking.

3.3. Structural characterization of the coatings

The structural characterization of the prepared coatings was made by FTIR spectroscopy. Fig. 6a displays the FTIR spectra of the liquid precursor mixtures before curing. As can be seen from Fig. 6a both TD3SH and TD4SH have similar spectra. The main bands to note in these spectra are the characteristic sharp azide stretching vibration band at 2100 cm^{-1}, the carbonyl bands at around 1720 cm^{-1}, and the allyl band at 1638 cm^{-1}. After the first curing step (UV irradiation), the allyl bands at 1638 cm^{-1} almost disappeared (Fig. 6b). As evident from the FTIR spectra of the fully cured coatings (Fig. 6c), the azide units had reacted with the remaining alkyne groups. After the thermal azide-alkyne click reactions the azide stretching vibration bands at 2100 cm^{-1} almost completely disappeared. These results show that the coatings were successfully prepared by combining TEP and azide-alkyne click reactions. We calculated the azide conversion percentage from the initial (Fig. 6a) and the final (Fig. 6c) absorbance values of the azide stretching vibration bands. The azide conversion percentages were found as 93.5% and 90.5% for TD3SH and TD4SH, respectively. It was previously reported that the azide groups do not completely react with the alkynes in copper-free thermal azide-alkyne click reactions [59,60]. Nevertheless, it can be said that these conversion percentages are high. The relatively lower azide conversion in the case of TD4SH can be attributed to its higher initial crosslink density.

We further evaluated the efficiency of our strategy to prepare eugenol-based coatings by measuring the extent of curing by calculating the gel-content values. We measured the gel-content values of the free films after both stages of curing (Table 1). Before the thermal treatment, the gel contents of the coatings were found to be 58%±3 and 56%±4 for TD3SH and TD4SH, respectively. After the thermal curing, the gel contents of the coatings increased to 96%±1 and 95%±2, for TD3SH and TD4SH, respectively. This finding clearly demonstrates that the azide-alkyne click reactions as well as siloxane hydrolysis and condensation reactions took place.

3.4. Light transmittance of the coatings

As can be seen from the images of the coatings given in Fig. 5, both TDSH3 and TDSH4 coatings were transparent. We evaluated the transparency of the coatings by measuring the light transmission percentage in the visible region. Fig. 7 displays the light transmission percentages of the coatings with respect to the wavelength. While TD3SH encoded coating exhibited almost 100% light transmittance between 800 and 500 nm, TD4SH displayed a gradually decreasing light transmittance in the same range. Nevertheless, even at 500 nm the light transmittance for TD4SH was ~ 90%. This slight difference between TD3SH and TD4SH can be attributed to the relatively more homogeneous network formation in the case of TD3SH. It is expected to have a much more flexible network with a lower degree of crosslinking when 3SH is used compared to the use of 4SH. Thus, the relatively flexible nature of TD3SH with respect to the TD4SH (owing to the lower crosslinking density) allowed a much more uniform siloxane network formation during the thermal curing process. Therefore, the more homogeneous TD3SH coatings resulted in much more transparent coatings.

3.5. Thermal properties of the coatings

The thermal stability of the coatings was investigated by TGA under nitrogen atmosphere. The TGA thermograms of the coatings are given in Fig. 8 and the TGA results are listed in Table 2. Both coating formulations displayed similar thermal degradation profiles under nitrogen atmosphere. All coatings were found to be thermally stable up to 200 °C, after this temperature all coatings gradually started to decompose. While TD3SH displayed a slightly lower 5% weight loss temperature ($T_{5\%}$), 10% weight loss temperature ($T_{10\%}$), and maximum weight loss temperature (T_{max}) than TD4SH, both coatings displayed similar char yields. $T_{5\%}$ and $T_{10\%}$ weight losses correspond to the unreacted monomers, ethanol, and water, which might form at higher temperatures due to further condensation of the unreacted silanol and alkoxy silane groups, and photoinitiator residues. The T_{max} values were found to be around 340 °C. The high T_{max} temperatures as well as the obtained high char yields (~35%) indicate that the coatings are thermally stable. When a diallyl compound derived from eugenol was cured with 3SH, the char yield of the resulting network at 600 °C was reported to be 7.1% [58]. Liu et al. prepared flame retardant networks by using a *hexa*-eugenol-substituted phosphazene monomer (HEP) [61]. This monomer was cured with different thiols via TEP and the properties of the resulting thermosets were evaluated. The results revealed that under nitrogen atmosphere, the char yields at 600 °C for 3SH and 4SH cured networks were below 35%. It can be said that the synergistic effect of the P, N, and Si atoms, the formation of the triazole rings, and the siloxane network led to highly thermally stable coatings in this study when compared to the literature.

The LOI values of the coatings were calculated according to Eq. (1). All formulations displayed LOI values above 30% (Table 2), indicating a high degree of flame retardancy. This result stems from the synergistic effect of P, N, and Si atoms. Generally, P-based flame retardants generate phosphoric acid-like species which lead to the early degradation of the polymer matrix and as a result a carbonaceous char forms. When nitrogen-based compounds are also present, they generate volatile species like ammonia which in turn causes the carbonaceous char to swell and form a foam-like dense char. This foam-like char impedes the transfer of heat and oxygen to layers below and as a result, the flame subsides. Besides, the formed species like ammonia dilute the oxygen

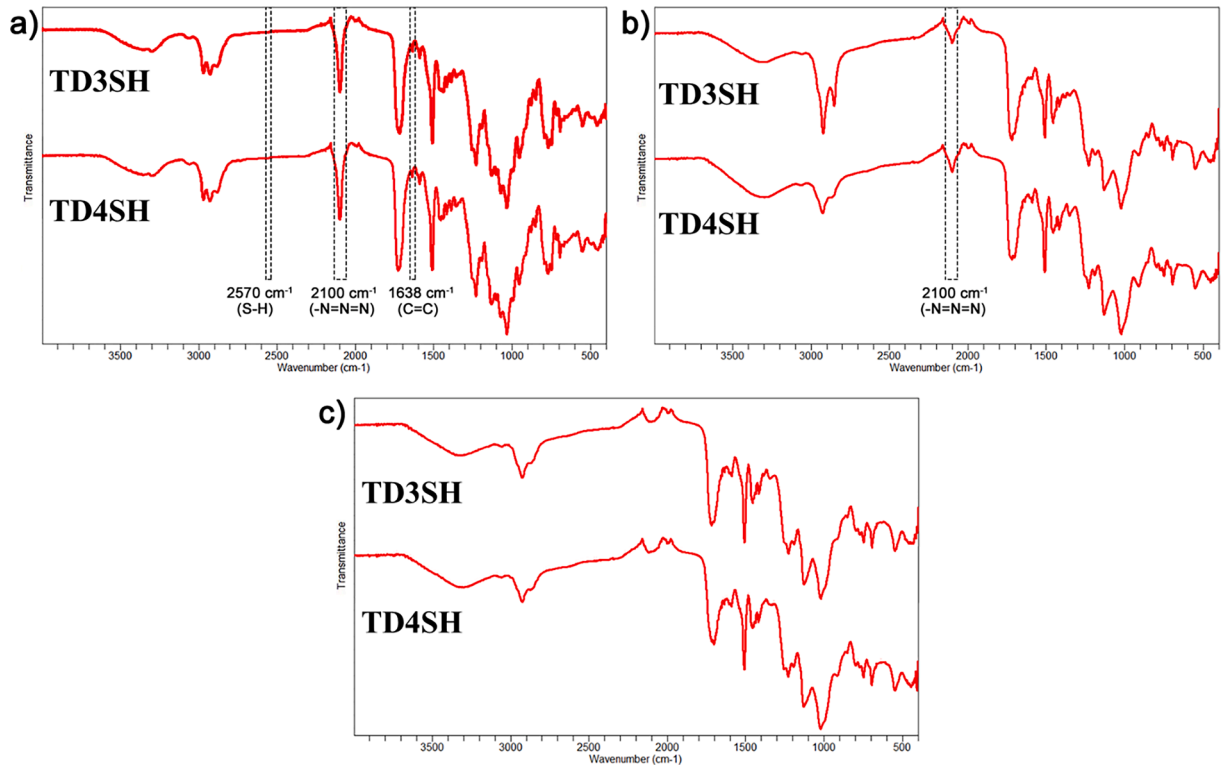

Fig. 6. FTIR spectra of TD3SH and TD4SH: a) liquid precursors, b) after UV curing, and c) after thermal curing.

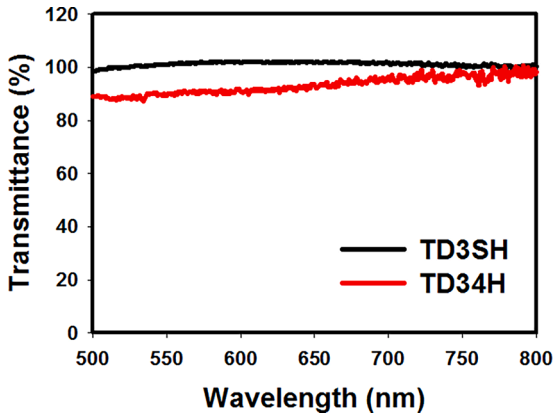

Fig. 7. Visible light transmittance of the coating formulations.

concentration in the gas phase, thereby aiding flame retardancy. Some of the phosphorous compounds also act in the gas phase and generate radicals that entrap oxygen radicals. The presence of glassy siloxane networks stabilizes the carbonaceous char and synergistically enhances flame retardancy.

We also detected the glass transition temperatures (T_gs) of the prepared thermosets via DSC measurements (Table 1). The T_g values were obtained from the second heating curves. Generally, the T_gs of thiol-ene photocured systems are low due to the flexible nature of the thioether bonds. Here, owing to the highly crosslinked structure and the presence of the rigid triazole units as well as the siloxane network, higher T_gs can be anticipated and to our expectation, the T_gs of the TD3SH and TD4SH were found as high as 76 °C and 94 °C, respectively. The increased T_g when 4SH was used, was attributed to the increased crosslinking density.

3.6. Surface wettability properties

The hydrophilic-hydrophobic character of the coatings was investigated by measuring the water contact angles. The results are plotted in Fig. 9 along with images that were taken from the Kruss software. The water contact angle of TD3SH was found to be 72 ± 3° while it was determined as 84 ± 2° for TD4SH. These results show that the coatings are hydrophilic. The presence of the polar phosphate groups hydrolyzed but uncondensed silanol groups and polar triazole units led to the observed hydrophilicity. The slightly increased water contact angle of the TD4SH was attributed to the contribution of the relatively hydrophobic 4SH compound and also to the increased crosslinking density. Similarly, Xue et al. attributed the increased contact angles of the thermoset resins to the increased crosslinking density, obtained by reacting 3SH or 4SH compounds with various allyl-terminated precursors derived from eugenol [62].

3.7. Coating performance tests

The physical properties of the dual-cured coatings are presented in Table 3. One of the most crucial properties of coatings that need to be examined is the extent of adhesion of the coating. The adhesion quality of the coatings applied onto glass substrates was tested via the crosscut test. According to this test, adhesion is classified from 0 (good adhesion) to 5 (poor adhesion). In this work, both the TD3SH and TD4SH coatings displayed excellent adhesion to the glass substrates and the level of adhesion was classified as 0 (Table 3). This good adhesion can be attributed to the presence of the siloxane and silanol groups which can covalently bond with the glass surface. Moreover, triazole groups can form H-bonding with the –OH groups on the surface of the glass substrate. Additionally, the polar phosphate units are also known to enhance adhesion. Dai et al., synthesized methacrylate-functionalized eugenol derivatives that bear polar –OH groups, mixed them with an acrylated vegetable oil and prepared UV-cured coatings [63]. The adhesion of their coatings increased with an increasing amount of the

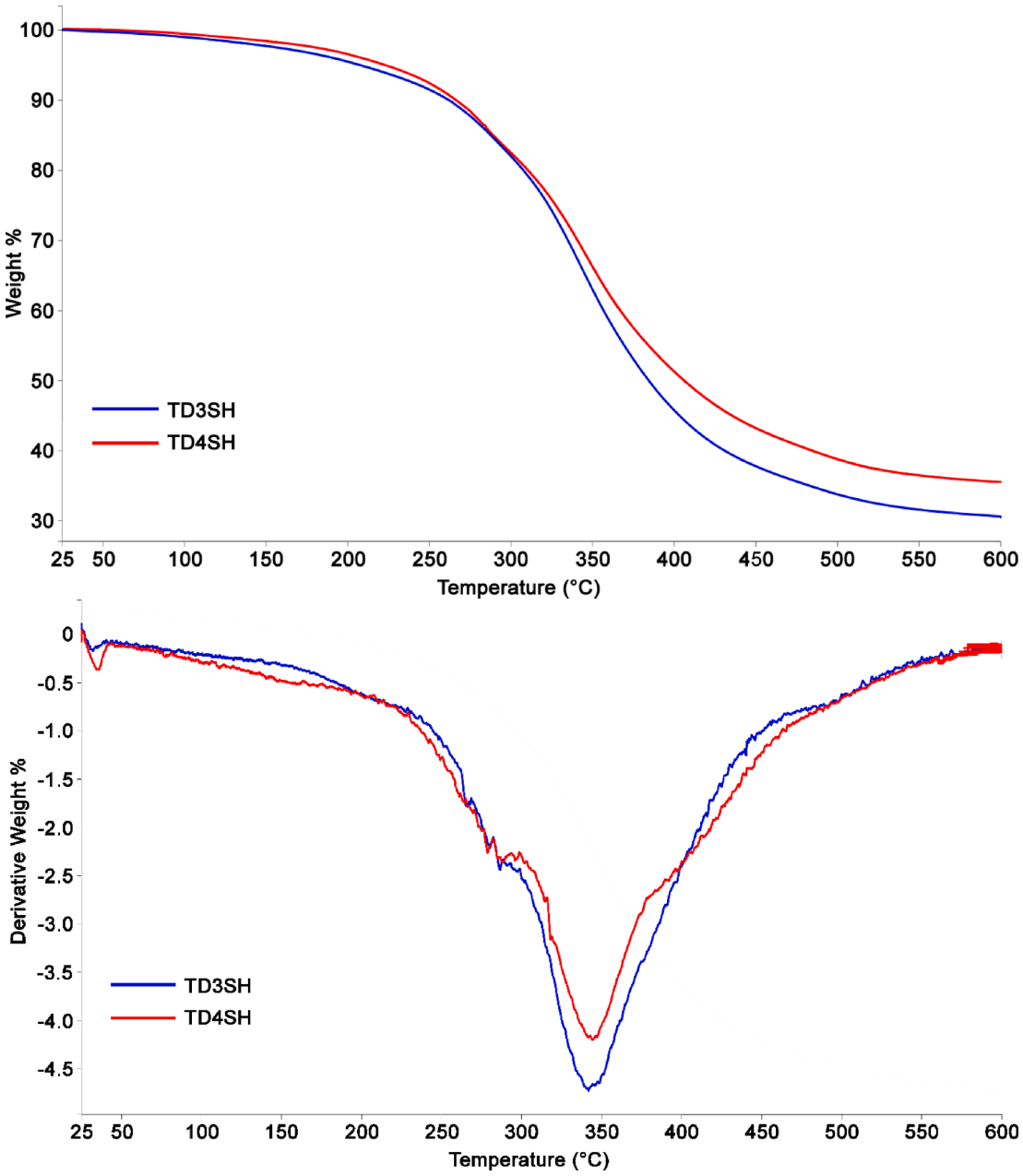

Fig. 8. TGA thermograms and the corresponding derivative weight curves of the coatings.

Table 2
TGA results of the coatings.

	$T_{5\%}$	$T_{10\%}$	T_{max}	Char yield	Theoretical LOI	T_g (°C)
TD3SH	208	262	342	35	31.0	76
TD4SH	220	265	345	34	30.6	94

eugenol derivatives and they stated that polar groups contribute positively to adhesion, leading to relatively improved adhesive forces.

Surface hardness of the dual-cured coatings was determined via pencil and pendulum hardness tests. The pencil hardness of the TD3SH and TD4SH coatings were found as 3H and 4H, respectively (Table 3). The increased pencil hardness of the TD4SH encoded coatings was attributed to the increased crosslinking degree due to the use of the four-functional thiol compound. The coatings prepared by Dai et al. displayed up to 2H pencil hardness values [63]. This shows that the

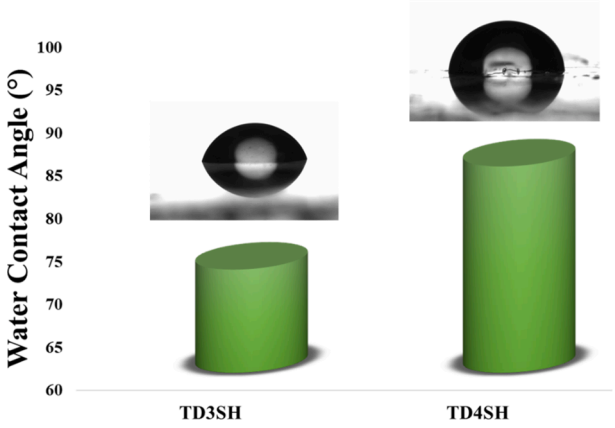

Fig. 9. WCA values of the coatings.

Table 3
Performance test results of the coatings.

	Cross-cut	Pencil Hardness	Pendulum Hardness	Gloss (Gloss Unit)		MEK rubbings	Water absorption (%)
				20°	60°		
TD3SH	0	3H	42 ± 4	137	138	250+	4.76
TD4SH	0	4H	65 ± 3	100	117	250+	4.01

inorganic–organic hybrid nature of our coatings improved the hardness values. Pendulum hardness test measures the damping capacity of the pendulum's oscillation by the coating. Softer coatings lead to shorter damping times while hard coatings result in higher oscillation times [64]. Again, the TD4SH was found to have a higher pendulum hardness than TD3SH due to its high degree of crosslinking (Table 3).

Gloss is the quantity of how shiny a surface is [65,66]. As shown in Table 3, the gloss of coatings, at 20° was measured to be 137 and 100 and at 60° as 138 and 117, for TD3SH and TD4SH, respectively.

The solvent resistance of coatings was evaluated by the MEK rubbing test. After 250 rubs, the appearance of the surface of the coatings did not alter. There was not a significant change observed in the coatings. Besides, the gloss values were found to be similar to the values measured before the MEK rubbing test. Furthermore, the chemical resistance of the coatings was investigated by dripping various reagents on the coated glass substrates (10% NaOH, 10% HCl, 10% H_2SO_4, and xylene) for 24 h. All coatings were found to be resistant to all the reagents used, no staining was observed on the surface of the coatings, and the general appearance of the samples was fine.

Finally, the water absorption percentages of the coatings were determined. Due to its relatively more crosslinked network, the water absorption percentage of the TD4SH was found to be less than TD3SH. Thus, it can be concluded that the swelling of the coatings was improved by increasing the functionality of the thiol component. Modjinou et al., prepared thiol-ene photocured coatings by using allyl-eugenol; a difunctional eugenol derivative [67]. They determined the water uptake percentage of the coating and found it to be 0.34%. The contact angle of the coating was 83° which was comparable to our coatings, yet, the water uptake values of our coatings were very high. Note that the method for the water uptake measurement in the study by Modjnou et al., is different than this work. Nevertheless, the high water uptake in our case might be attributed to the presence of the polar and hydrophilic groups in the structure of the synthesized materials.

4. Conclusions

In this work, we synthesized a novel, eugenol-based monomer containing P, N, and Si atoms. Even though we fully characterized this monomer, its low yield led us to an elegant pathway that involved the application of a dual curing system. The dual-curing strategy utilized in this work combined two modern chemical techniques; TEP and azide-alkyne click reactions.

While the thinner coatings (<100 μm) were found to be colorless and highly transparent to visible light, thicker coatings were yellowish (>200 μm). The coatings displayed high thermal stability, as evidenced by the char yields at 600 °C, and displayed good resistance to solvents, acidic and basic reactants. The prepared materials herein can be used for the preparation of the floor, furniture, wood, textile, glass, leather coatings, etc. Especially, the developed dual-cured thermoset can be suitable to coat wood furniture with the benefit of improved thermal stability.

We believe that this work demonstrates an example of an innovative, thermally stable coating preparation that promises modern chemical pathways within the framework of green chemistry. We also believe that more work will be carried out in the future combining bio-based building blocks with modern click chemistry protocols to prepare smart and functional materials.

CRediT authorship contribution statement

Ozge Ozukanar: Investigation, Writing – original draft. **Emrah Çakmakçi:** Investigation, Conceptualization, Writing – original draft. **Ozgun Daglar:** Investigation. **Hakan Durmaz:** Conceptualization, Methodology. **Volkan Kumbaraci:** Investigation, Conceptualization, Writing – original draft.

Declaration of Competing Interest

The authors declare that they have no known competing financial interests or personal relationships that could have appeared to influence the work reported in this paper.

Data availability

Data will be made available on request.

Acknowledgment

This work was supported by the Scientific Research Projects Department of Istanbul Technical University (ITU-BAP) (Project number: TGA-2022-43637).

Appendix A. Supplementary data

Supplementary data to this article can be found online at https://doi.org/10.1016/j.eurpolymj.2023.112203.

References

[1] L. Qin, Y. He, B. Liu, Y. Jian, C. Li, J. Nie, Preparation and properties of polyurethane acrylates modified by saturated alcohols, Prog. Org. Coat. 76 (2013) 1594–1599, https://doi.org/10.1016/j.porgcoat.2013.07.005.
[2] E. Dzunuzovic, S. Tasic, B. Bozic, D. Babic, B. Dunjic, UV-curable hyperbranched urethane acrylate oligomers containing soybean fatty acids, Prog. Org. Coat. 52 (2005) 136–143, https://doi.org/10.1016/j.porgcoat.2004.10.003.
[3] Y. Mülazim, E. Çakmakçı, M.V. Kahraman, Preparation of photo curable highly hydrophobic coatings using a modified castor oil derivative as a sol–gel component, Prog. Org. Coat. 72 (2011) 394–401, https://doi.org/10.1016/j.porgcoat.2011.05.012.
[4] R. Chandra, R.K. Soni, Recent developments in thermally curable and photocurable systems, Prog. Polym. Sci. 19 (1994) 137–169, https://doi.org/10.1016/0079-6700(94)90039-6.
[5] H. Seker, E. Çakmakçi, Fully bio-based thiol-ene photocured thermosets from isosorbide and tung oil, J. Polym. Sci. 58 (2020) 1105–1114, https://doi.org/10.1002/pol.20190291.
[6] Y. Mülazim, E. Çakmakçı, M.V. Kahraman, Photo-curable highly water-repellent nanocomposite coatings, J. Vinyl Addit. Technol. 19 (2013) 31–38, https://doi.org/10.1002/vnl.20309.
[7] J. Fu, L. Wang, H. Yu, M. Haroon, F. Haq, W. Shi, B. Wu, L. Wang, Research progress of UV-curable polyurethane acrylate-based hardening coatings, Prog. Org. Coat. 131 (2019) 82–99, https://doi.org/10.1016/j.porgcoat.2019.01.061.
[8] E. Çakmakçı, Allylamino diphenylphosphine oxide and poss containing flame retardant photocured hybrid coatings, Prog. Org. Coat. 105 (2017) 37–47, https://doi.org/10.1016/j.porgcoat.2016.11.013.
[9] D. Hagood, M. Kelly, Extolling the advantages of UV-curing processes, Metal Finish. 106 (2008) 71–74, https://doi.org/10.1016/S0026-0576(08)80098-0.
[10] S.C. Ligon, B. Husár, H. Wutzel, R. Holman, R. Liska, Strategies to reduce oxygen inhibition in photoinduced polymerization, Chem. Rev. 114 (2014) 557–589, https://doi.org/10.1021/cr3005197.
[11] B. Husár, S.C. Ligon, H. Wutzel, H. Hoffmann, R. Liska, The formulator's guide to anti-oxygen inhibition additives, Prog. Org. Coat. 77 (2014) 1789–1798, https://doi.org/10.1016/j.porgcoat.2014.06.005.

[12] N.B. Cramer, T. Davies, A.K. O'Brien, C.N. Bowman, Mechanism and modeling of a thiol-ene photopolymerization, Macromolecules 36 (2003) 4631–4636, https://doi.org/10.1021/ma034072x.
[13] M.J. Kade, D.J. Burke, C.J. Hawker, The power of thiol-ene chemistry, J. Polym. Sci. Part A Polym. Chem. 48 (2010) 743–750, https://doi.org/10.1002/pola.23824.
[14] C.E. Hoyle, C.N. Bowman, Thiol-ene click chemistry, Angew. Chem. Int. Ed. 49 (2010) 1540–1573, https://doi.org/10.1002/anie.200903924.
[15] E. Cakmakcı, Y. Mülazim, M.V. Kahraman, N. Kayaman-Apohan, Flame retardant thiol-ene photocured coatings, React. Funct. Polym. 71 (2011) 36–41, https://doi.org/10.1016/j.reactfunctpolym.2010.11.011.
[16] D.P. Nair, N.B. Cramer, T.F. Scott, C.N. Bowman, R. Shandas, Photopolymerized thiol-ene systems as shape memory polymers, Polymer 51 (2010) 4383–4389, https://doi.org/10.1016/j.polymer.2010.07.027.
[17] T. Clark, L. Kwisnek, C.E. Hoyle, S. Nazarenko, Photopolymerization of thiol-ene systems based on oligomeric thiols, J. Polym. Sci., Part A: Polym. Chem. 47 (2009) 14–24, https://doi.org/10.1002/pola.23089.
[18] B.-S. Chiou, R.J. English, S.A. Khan, Rheology and Photo-Cross-Linking of Thiol−Ene Polymers, Macromolecules 29 (1996) 5368–5374, https://doi.org/10.1021/ma960383e.
[19] G. Sagdic, E. Cakmakci, O. Daglar, U.S. Gunay, G. Hizal, U. Tunca, H. Durmaz, Thermal and mechanical properties of thiol-ene photocured thermosets containing DOPO-based liquid reactive flame retardant synthesized by metal-free azide-alkyne click reaction, Prog. Org. Coat. 167 (2022), 106825, https://doi.org/10.1016/j.porgcoat.2022.106825.
[20] L. Pezzana, G. Melilli, P. Delliere, D. Moraru, N. Guigo, N. Sbirrazzuoli, M. Sangermano, Thiol-ene biobased networks: Furan allyl derivatives for green coating applications, Prog. Org. Coat. 173 (2022), 107203, https://doi.org/10.1016/j.porgcoat.2022.107203.
[21] L. Pezzana, M. Sangermano, Fully biobased UV-cured thiol-ene coatings, Prog. Org. Coat. 157 (2021), 106295, https://doi.org/10.1016/j.porgcoat.2021.106295.
[22] B. Oktay, E. Çakmakci, DOPO tethered Diels Alder clickable, reactive silica nanoparticles for bismaleimide containing flame retardant thiol-ene nanocomposite coatings, Polymer 131 (2017) 132–142, https://doi.org/10.1016/j.polymer.2017.10.043.
[23] O. Daglar, E. Çakmakçi, U.S. Gunay, G. Hizal, U. Tunca, H. Durmaz, Acetylene Dicarboxylic Acid Diallyl Ester: A Versatile Monomer for Thiol-Ene Photocured Networks, Macromol. Mater. Eng. 306 (2021) 2100427, https://doi.org/10.1002/mame.202100427.
[24] E. Çakmakçı, Y. Mülazim, M.V. Kahraman, N.K. Apohan, Preparation and characterization of boron containing thiol–ene photocured hybrid coatings, Prog. Org. Coat. 75 (2012) 28–32, https://doi.org/10.1016/j.porgcoat.2012.03.003.
[25] H. Xu, X. Bao, F. Wu, J. Wang, Effect of a Phosphorus-Silicon Containing Flame Retardant on the Activation Energy in Thermal Degradation of Thiol-ene Composites, Russ. J. Appl. Chem. 94 (2021) 1002–1008, https://doi.org/10.1134/S1070427221070193.
[26] C. Cheng, X. Zhang, X. Chen, J. Li, Q. Huang, Z. Hu, Y. Tu, Self-healing polymers based on eugenol via combination of thiol-ene and thiol oxidation reactions, J. Polym. Res. 23 (2016) 1–12, https://doi.org/10.1007/s10965-016-1001-x.
[27] M. Shibata, N. Tetramoto, A. Imada, M. Neda, S. Sugimoto, Bio-based thermosetting bismaleimide resins using eugenol, bieugenol and eugenol novolac, React. Funct. Polym. 73 (2013) 1086–1095, https://doi.org/10.1016/j.reactfunctpolym.2013.05.002.
[28] K. Hu, D. Zhao, G. Wu, J. Ma, Polyesters derived from bio-based eugenol and 10-undecenoic acid: synthesis, characterization, and structure–property relationships, RSC Adv. 5 (2015) 85996–86005, https://doi.org/10.1039/C5RA17457K.
[29] E. Cakmakci, F. Sen, M.V. Kahraman, Isosorbide Diallyl Based Antibacterial Thiol-Ene Photocured Coatings Containing Polymerizable Fluorous Quaternary Phosphonium Salt, ACS Sustain. Chem. Eng. 7 (2019) 10605–10615, https://doi.org/10.1021/acssuschemeng.9b01161.
[30] Y. Çakmak, E. Çakmakçi, N.K. Apohan, R. Karadag, Isosorbide, pyrogallol, and limonene-containing thiol-ene photocured bio-based organogels for the cleaning of artworks, J. Cult. Heritage 55 (2022) 391–398, https://doi.org/10.1016/j.culher.2022.04.013.
[31] S. Doran, E. Murtezi, F.B. Barlas, S. Timur, Y. Yagci, One-pot photo-induced sequential CuAAC and thiol–ene click strategy for bioactive macromolecular synthesis, Macromolecules 47 (2014) 3608–3613, https://doi.org/10.1021/ma5007039.
[32] B. Iskin, G. Yilmaz, Y. Yagci, ABC type miktoarm star copolymers through combination of controlled polymerization techniques with thiol-ene and azide-alkyne click reactions, J. Polym. Sci., Part A: Polym. Chem. 49 (2011) 2417–2422, https://doi.org/10.1002/pola.24672.
[33] G.O. Eyrilmez, S. Doran, E. Murtezi, B. Demir, D.O. Demirkol, H. Coskunol, S. Timur, Y. Yagci, Selective Cell Adhesion and Biosensing Applications of Bio-Active Block Copolymers Prepared by CuAAC/Thiol-ene Double Click Reactions, Macromol. Biosci. 15 (2015) 1233–1241, https://doi.org/10.1002/mabi.201500099.
[34] H. Naguib, X. Cao, H. Gao, Synthesize Hyperbranched Polymers Carrying Two Reactive Handles via CuAAC Reaction and Thiol-Ene Chemistry, Macromol. Chem. Phys. 220 (2019) 1900221, https://doi.org/10.1002/macp.201900221.
[35] P. Antoni, M.J. Robb, L. Campos, M. Montanez, A. Hult, E. Malmstrom, M. Malkoch, C.J. Hawker, Pushing the limits for thiol− ene and CuAAC reactions: Synthesis of a 6th generation dendrimer in a single day, Macromolecules 43 (2010) 6625–6631, https://doi.org/10.1021/ma101242u.
[36] K. Öberg, Y. Hed, I.J. Rahmn, J. Kelly, P. Löwenhielm, M. Malkoch, Dual-purpose PEG scaffolds for the preparation of soft and biofunctional hydrogels: the convergence between CuAAC and thiol–ene reactions, Chem. Commun. 49 (2013) 6938–6940, https://doi.org/10.1039/C3CC42084A.
[37] A.S. Goldmann, A. Walther, L. Nebhani, R. Joso, D. Ernst, K. Loos, C. Barner-Kowollik, A.H. Müller, Surface modification of poly (divinylbenzene) microspheres via thiol− ene chemistry and alkyne− azide click reactions, Macromolecules 42 (2009) 3707–3714, https://doi.org/10.1021/ma900332d.
[38] J. Iehl, J.F. Nierengarten, Sequential copper catalyzed alkyne–azide and thiol–ene click reactions for the multiple functionalization of fullerene hexaadducts, Chem. Commun. 46 (2010) 4160–4162, https://doi.org/10.1039/C0CC00252F.
[39] A.A. Alzahrani, D.P. Nair, D.J. Smits, M. Saed, C.M. Yakacki, C.N. Bowman, Photo-CuAAC Induced Wrinkle Formation in a Thiol-Acrylate Elastomer via Sequential Click Reactions, Chem. Mater. 26 (2014) 5303–5309, https://doi.org/10.1021/cm502237b.
[40] S. Mestry, P. Borse, M. Patil, S. Vaidya, S. Jadhav, S.T. Mhaske, Vanillin-derived phosphorus-containing aromatic imine for flame-retardant polyurethane coating, Iran. Polym. J. 31 (2022) 1183–1196, https://doi.org/10.1007/s13726-022-01065-5.
[41] B. Iskin, G. Yilmaz, Y. Yagci, Synthesis of ABC type miktoarm star copolymers by triple click chemistry, Polym. Chem, Chemistry 12 (2011) 2865–2871, https://doi.org/10.1039/C1PY00352F.
[42] B. Liu, J. Chen, N. Liu, H. Ding, X. Wu, B.D. Kim, Bio-based polyesters synthesized by ring-opening copolymerizations of eugenyl glycidyl ether and cyclic anhydrides using a binuclear [OSSO]CrCl complex, Green Chem. 22 (2020) 5742–5750, https://doi.org/10.1039/D0GC00469C.
[43] O. Ozukanar, E. Çakmakçi, G. Sagdic, U.S. Gunay, H. Durmaz, V. Kumbaraci, Eugenol-DOPO: A Bio-Based Phosphorous-Containing Monomer for Thiol-ene Photocurable Thermosets, J. Polym. Environ. (2023) 1–13, https://doi.org/10.1007/s10924-023-02813-1.
[44] V.G. Isoppo, M.O. Rodrigues, F.S. Rodembusch, A.V. Moro, 2, 1, 3-Benzothiadiazole-based bis-silylated compounds: Synthesis and use in the preparation of highly fluorescent low-contend organic–inorganic hybrid materials, J. Photochem. Photobiol., A 435 (2023), 114277, https://doi.org/10.1016/j.jphotochem.2022.114277.
[45] I. Faye, M. Decostanzi, Y. Ecochard, S. Caillol, Eugenol bio-based epoxy thermosets: from cloves to applied materials, Green Chem. 19 (2017) 5236–5242, https://doi.org/10.1016/j.jphotochem.2022.114277.
[46] V. Fındık, B.T. Varinca, I. Degirmenci, S.S. Erdem, Insight into the Thiol-yne Kinetics via a Computational Approach, J. Phys. Chem. A 125 (2021) 3556–3568, https://doi.org/10.1021/acs.jpca.0c11599.
[47] V. Fındık, I. Degirmenci, Ş. Çatak, V. Aviyente, Theoretical investigation of thiol-ene click reactions: A DFT perspective, Eur. Polym. J. 110 (2019) 211–220, https://doi.org/10.1016/j.eurpolymj.2018.11.030.
[48] B.D. Fairbanks, T.F. Scott, C.J. Kloxin, K.S. Anseth, C.N. Bowman, Thiol− yne photopolymerizations: Novel mechanism kinetics, and step-growth formation of highly cross-linked networks, Macromolecules 42 (2009) 211–217, https://doi.org/10.1021/ma801903w.
[49] R. Gómez-Balderas, M.L. Coote, D.J. Henry, H. Fischer, L. Radom, What is the origin of the contrathermodynamic behavior in methyl radical addition to alkynes versus alkenes? J. Phys. Chem. A 107 (2003) 6082–6090, https://doi.org/10.1021/jp035042z.
[50] R. Gómez-Balderas, M.L. Coote, D.J. Henry, L. Radom, Reliable theoretical procedures for calculating the rate of methyl radical addition to carbon− carbon double and triple bonds, J. Phys. Chem. A 108 (2004) 2874–2883, https://doi.org/10.1021/jp036375z.
[51] M. Ciftci, M.U. Kahveci, Y. Yagci, X. Allonas, C. Ley, H. Tar, A simple route to synthesis of branched and cross-linked polymers with clickable moieties by photopolymerization, Chem. Commn. 48 (2012) 10252–10254, https://doi.org/10.1039/C2CC35607D.
[52] M.B. Bilgic, K. Kaya, N. Orakdogen, Y. Yagci, Light-induced synthesis and characterization of "Clickable" polyacrylamide hydrogels, Eur. Polym. J. 16 (167) (2022), 111062, https://doi.org/10.1016/j.eurpolymj.2022.111062.
[53] S. Santra, R. Bean, B. Heckert, Z. Shaw, V. Jain, L. Shrestha, R. Narayanam, Q. Austin, Alkene–azide chemistry: A facile, one-step, solvent-and catalyst-free approach for developing new functional monomers and polymers, Polym. Chem. 11 (2020) 3723–3731, https://doi.org/10.1039/D0PY00346H.
[54] N. Naga, H. Nagino, H. Furukawa, Synthesis of organic-inorganic hybrid gels by means of thiol-ene and azide-alkene reactions, J. Polym. Sci., Part A: Polym. Chem. 54 (2016) 2229–2238, https://doi.org/10.1002/pola.28096.
[55] D. Damiron, N. Okhay, S.A. Akhrass, P. Cassagnau, E. Drockenmuller, Crosslinked PDMS elastomers and coatings from the thermal curing of vinyl-functionalized PDMS and a diazide aliphatic crosslinker, J. Polym. Sci., Part A: Polym. Chem. 50 (2012) 98–107, https://doi.org/10.1002/pola.24991.
[56] T. Yoshimura, T. Shimasaki, N. Teramoto, M. Shibata, Bio-based polymer networks by thiol–ene photopolymerizations of allyl-etherified eugenol derivatives, Eur. Polym. J. 67 (2015) 397–408, https://doi.org/10.1016/j.eurpolymj.2014.11.013.
[57] D. Guzman, X. Ramis, X. Fernandez-Francos, S. De la Flor, A. Serra, New bio-based materials obtained by thiol-ene/thiol-epoxy dual curing click procedures from eugenol derivates, Eur. Polym. J. 93 (2017) 530–544, https://doi.org/10.1016/j.eurpolymj.2017.06.026.
[58] J. Dai, S. Ma, L. Zhu, S. Wang, L. Yang, Z. Song, X. Li, J. Zhu, uV-thermal dual cured anti-bacterial thiol-ene networks with superior performance from renewable resources, Polymer 108 (2017) 215–222, https://doi.org/10.1016/j.polymer.2016.11.068.
[59] E. Çakmakçı, M. Özdemir, F. Şen, M. Bulut, B. Yalçın, Vegetable oil-based, coumarin-containing antibacterial thermosets with improved thermal stability via

copper-free thermal azide-alkyne click polymerization, Ind. Crops Prod. 182 (2022), 114870, https://doi.org/10.1016/j.indcrop.2022.114870.
[60] Y. Han, L. Yuan, G. Li, L. Huang, T. Qin, F. Chu, C. Tang, Renewable polymers from lignin via copper-free thermal click chemistry, Polymer 83 (2016) 92–100, https://doi.org/10.1016/j.polymer.2015.12.010.
[61] T. Liu, L. Sun, R. Ou, Q. Fan, L. Li, C. Guo, Z. Liu, Q. Wang, Flame retardant eugenol-based thiol-ene polymer networks with high mechanical strength and transparency, Chem. Eng. J. 368 (2019) 359–368, https://doi.org/10.1016/j.cej.2019.02.200.
[62] J. Xue, X. Yang, Y. Ke, Z. Yan, X. Dong, Y. Luo, C. Zhang, Novel eugenol-based allyl-terminated precursors and their bio-based polymer networks through thiol-ene click reaction, Ind. Crops Prod. 171 (2021), 113956, https://doi.org/10.1016/j.indcrop.2021.113956.
[63] J. Dai, Y. Jiang, X. Liu, J. Wang, J. Zhu, Synthesis of eugenol-based multifunctional monomers via a thiol–ene reaction and preparation of UV curable resins together with soybean oil derivatives, RSC Adv. 6 (2016) 17857–17866, https://doi.org/10.1039/C6RA01420H.
[64] Z. Altıntaş, E. Çakmakçı, M.V. Kahraman, N.K. Apohan, A. Güngör, Preparation of photocurable silica–titania hybrid coatings by an anhydrous sol–gel process, J. Sol-Gel Sci. Technol. 58 (2011) 612–618, https://doi.org/10.1007/s10971-011-2435-6.
[65] C. Zha, X. Luo, R. Wang, B. Luther-Davies, Effects of TiO2 and ZrO2 on optical properties of organic–inorganic hybrid polymers and thin films, J. Mater. Sci. Mater. Electron. 18 (2007) 331–334, https://doi.org/10.1007/s10854-007-9216-6.
[66] E. Cakmakcı, Z. Altıntaş, M.V. Vezir Kahraman, N.K. Apohan, Fluorine-containing photocurable hybrid coatings via anhydrous sol–gel method, J. Vinyl Add. Tech. 21 (2015) 272–277, https://doi.org/10.1002/vnl.21398.
[67] T. Modjinou, H. Rodriguez-Tobias, G. Morales, D.L. Versace, V. Langlois, D. Grande, E. Renard, UV-cured thiol–ene eugenol/ZnO composite materials with antibacterial properties, RSC Adv. 6 (2016) 88135–88142, https://doi.org/10.1039/C6RA18551G.